A combined dynamic simulation and experimental study on the performance of the adsorbed natural gas system under variable charging conditions

Shohreh Mirzaei[1,2], Akbar Shahsavand[1,2,*], Ali Ahmadpour[1,2], Ali Garmroodi Asil[3], Arash Arami-Niya[4,*]

[1] Department of Chemical Engineering, Faculty of Engineering, Ferdowsi University of Mashhad, P.O. Box 91779-48944, Mashhad, Iran.

[2] Research Laboratory of Adsorbents and Catalysts, Research Institute of Oil & Gas, Ferdowsi University of Mashhad, Mashhad, Iran.

[3] Department of Chemical Engineering, Faculty of Engineering, University of Bojnord, Bojnord, Iran.

[4] Discipline of Chemical Engineering, Western Australian School of Mines: Minerals, Energy and Chemical Engineering, Curtin University, GPO Box U1987, Perth, WA 6845, Australia.

Abstract

Adsorbed natural gas (ANG) technology is considered a cost-effective and sustainable energy storage system that can offer a leading energy source to meet present demands for clean and environmentally friendly combustion fuel. Despite the benefits of ANG systems, still, there are some challenges in accurate simulation of these systems to analyse their performance under actual conditions. Here, the actual charging condition of ANG vessel with variable gas flow rate was simulated and experimentally validated for the first time. For this purpose, we proposed a new time-dependent equation to monitor methane's variable injection flow rate into the vessel. Dynamic CH_4 storage was experimentally tested to validate the simulation results using a custom-built pressurised ANG vessel (~300 cm^3) filled with two various in-house prepared adsorbents (i.e. AC1 and AC2) under the loading condition of 40 bar and 25 °C. Also, the thermal behaviour of the ANG vessel was studied via experimental observations. A 2D distributed dynamic model, solved by COMSOL Multiphysics software, was developed to assist the simulation in predicting pressure and temperature variations inside the ANG bed. Analysis of the ANG vessel's

* Corresponding authors;
Tel: +98-51-38805124. Email: shahsavand@um.ac.ir
Tel: +61-8-9266 5482. Email: arash.araminiya@curtin.edu.au

performance exhibited higher thermal fluctuations attributed to the adsorbent with superior isothermal methane storage capacity. Due to the low thermal conductivity of both adsorbents, a significant temperature rise was observed in the central region of the bed. Sensitivity analysis shows that increasing the length and diameter of the ANG tank leads to a longer required time for charging the tank up to the desired pressure and relative decreases in the temperature profile. Moreover, increasing heat capacity of adsorbent from 800 to 1350 J/kg.K caused 37% reduction in the temperature variations and 7.7% enhancement in gravimetric methane storage efficiency.

Keywords: Adsorbed Natural Gas, thermal behaviour, adsorbents, dynamic simulation, sensitivity analysis.

Graphical Abstract

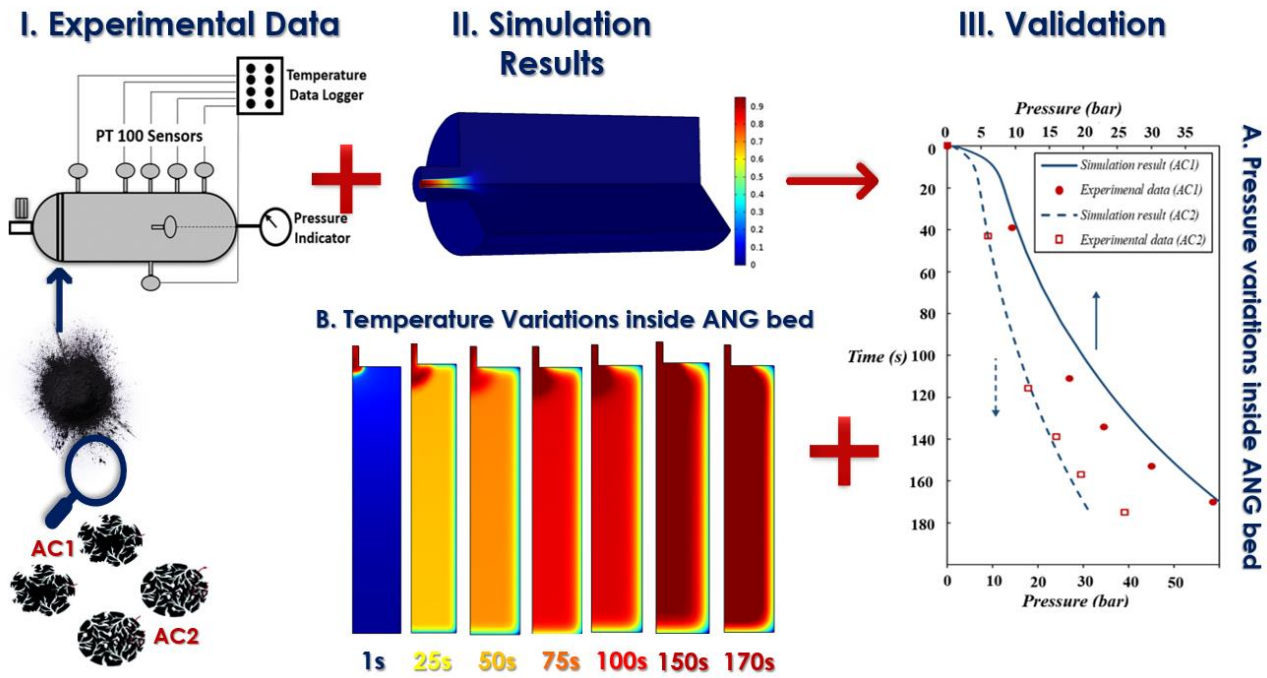

Nomenclature

Variables & constants

A	Polony's adsorption potential
A_{inlet}	Inlet surface area of gas opening (m^2)
C_p	Specific heat capacity at constant pressure (J/kg.K)
E_0	Activation energy (J/mol)
h_c	Convective heat transfer coefficient ($W/m^2.K$)
K	Permeability of the bed (m^2)
M	Molecular weight (kg/mol)
n	DA exponent
n'	Unit outward normal to the surface
P	Pressure (bar)
P_s	Saturation vapor pressure (bar)
q	Gravimetric amount of adsorbed gas (kg/kg)
Q_{ANG}	Inlet gas flow rate (L/s)
$\dot{Q}$	Heat flux (W/m^2)
r	Radial coordinate
R	Universal gas constant (J/mol.K)
t	Time (s)
T	Temperature (K)
v	Velocity (m/s)
V	Volume (cm^3)
V_t	Total pore volume of adsorbent (m^3/kg)
W_0	Maximum volumetric adsorbate uptake of the adsorbent (m^3/kg)
z	Axial direction
Z	Compressibility factor

Greek symbols

α	Thermal expansion coefficient (1/K)
β	Affinity coefficient
ΔH	Isosteric heat of adsorption (J/mol)
ΔN	Molar flow (mol/s)
ε	Porosity
λ	Thermal conductivity (W/m.K)
μ	Dynamic viscosity (kg/m.s)
ρ	Density (kg/m^3)
$\bar{\rho}$	Density of liquid methane at the Normal boiling point (kg/m^3)

Subscripts

ads	adsorbed
amb	Ambient condition
ave	Average
ANG	Adsorbed natural gas
b	Bed
B	Boiling
BHS	Boundary heat source
conv	Convective condition
cr	Critical point heat transfer
CNG	Compressed natural gas
d	Doser
eff	Effective
g	Gas
i	Initial
inlet	Inlet point condition
p	Particle
r	Radial direction
s	Solid
STP	Standard temperature and pressure
z	Axial direction

1. Introduction

Natural gas has been implemented as an alternative fuel source in recent years due to its local abundance and environmental benefits [1, 2]. Natural gas storage has predominately been conducted through compressed natural gas (CNG), liquefied natural gas (LNG) systems, and, more recently, adsorbed natural gas (ANG) [3]. For the CNG technology, natural gas is needed to compress up to around 200 bar pressure. Such high pressure is provided via a costly multi-stage compression process inside a high-strength storage vessel[1]. On the other hand, LNG is stored in a double-wall vacuum-insulated pressurised vessel to preserve the liquid form under -160 to - 196 °C. Therefore, the storage and management of LNG can be considered an energy and cost-intensive technique [2]. This storage method is only used as a vehicle fuel in heavy-duty, high fuel-demand vehicles such as highway trucks and construction equipment [3].

Adsorbed natural gas (ANG) systems have been proposed to increase natural gas's energy density at low pressures and room temperature. In the ANG systems, high surface area porous materials such as activated carbons (ACs), zeolites, metal-organic frameworks (MOFs), covalent organic frameworks (COFs), porous aromatic frameworks (PAFs) will be used to increase the system's storage capacity due to the increase in the natural gas's density near the surface of the adsorbents at any given pressure and temperature [6-9]. ANG process typically operates at room temperature and maximum pressures between 35 and 60 bar, significantly lower than the compression pressure of ~200 bar in CNG systems. The lower operating pressure and temperature mean that the cost of the designed vessels is affordable compared to others.

Despite the benefits of ANG systems, there are still significant challenges that need to be addressed, including packing of adsorbent material inside the ANG tank, managing flow rates during injection/consumption of gas, limited driving distance before refuelling and more

---

[1] The study on the economic feasibility associated with compressed natural gas vehicle fueling provide estimated cost range of $250000-$600000 for instalation of medium CNG station with capacity of 500-800 gasoline gallon equivalent per day.

[4] M. Smith, J. Gonzales, Costs associated with compressed natural gas vehicle fueling infrastructure, National Renewable Energy Lab.(NREL), Golden, CO (United States), 2014.

[2] The expenses of diffrent phase related to the LNG opetation are generally included exploration & production ($0.60–1.2 per one million British thermal units, or MMBtu), liquefaction ($0.90–1.30/MMBtu), shipping ($0.50–1.80/MMBtu), storage & regasification ($0.40–0.60/MMBtu).

[5] J. Cho, G.J. Lim, S.J. Kim, T. Biobaku, Liquefied natural gas inventory routing problem under uncertain weather conditions, International Journal of Production Economics 204 (2018) 18-29.

importantly, high fluctuations of tank's temperature due to the heat of adsorption which affect the system's storage capacity and dynamics [10-14]. Several experimental studies and theoretical modelling of ANG storage vessels have been made to investigate these imperfections [14-16]. Sáez et al. showed that the central region of the ANG bed suffers highly from temperature fluctuation during charge and discharge processes, which can be mitigated by improving the adsorbent's properties such as BET surface area [10]. A similar study revealed that using adsorbents with higher adsorption capacity results in a more extreme thermal fluctuation of about 99.2 °C at the bed centre [17]. The maximum temperature rise happens in the central region of the bed, mainly due to adsorbents' low thermal conductivity.

The development of theoretical tools to accurately describe ANG storage systems' dynamics with realistic geometries is another approach to assessing the ANG tanks' performances for the onboard storage vehicular. In 1997, Mota et al. theoretically studied various aspects of the dynamic storage system using AC as the adsorbent [18]. The proposed mathematical models include mass, momentum, and heat transfer equations to observe the thermal effects and hydrodynamics of flow through the carbon bed. The obtained results showed that during fast charging, ANG tanks suffer from severe thermal effects. Vasiliev et al. (2000) suggested a new type of multicell ANG vessel with internal heat pipes for better thermal control [19]. They analysed a new microporous adsorbent (active carbon fibre disks, produced from pyrolysis of Busofit) capable of delivering near 150 (V_{CH4}/V_{Bed}) after charging at 35 bar. They introduced a distributed model to predict the temperature profile during the radial gas discharge inside a cylindrical ANG vessel. The vessel was equipped with internal finned heaters for thermal control purposes. An ANG vessel (containing seven cylinders) with a total volume of 43000 cm^3 was used to gather the experimental desorption data. The model predictions of the ANG system’s performance were fairly in agreement with the measurement results.

Kazi *et al.* (2011) introduced a two-dimensional (2D) distributed model to simulate their custom-built ANG setup with internal fins and tubes at both charge and discharge conditions [20]. The simulations showed that the capacity of the charge and discharge processes was notably enhanced after the fins and tubes' insertion agreed with the experimental results. Khorashadizadeh *et al.* (2014) presented a model to mimic the discharge process of an ANG tank [21]. They compared the experimental data (borrowed from relevant research in the literature) with their prediction

results of the proposed lumped model. The simulation results indicated good agreement between the proposed model predictions and the validation data. In 2018, Patil *et al.* theoretically studied the ANG storage system's performance for different charging conditions (i.e. constant pressure and constant flow charging) [22]. Comparing the simulation results with their experimental data showed that the proposed model adequately considered the real gas properties of methane, variations of adsorbed phase properties, and the heat of adsorption.

In the real condition when an ANG capsule is being set, the inlet gas flow rate is not constant; it fills with its maximum input rate at the start of the charging process and the flow rate decreases due to the gradual increase in the storage vessel's pressure. The charging process terminates as the downstream pressure reaches a prespecified value. Thus, it is necessary to remark that during the experimental and theoretical investigations of ANG systems. The fluid properties during injection should be studied as time-dependent variables mainly due to the tank's pressure changes as the bed gets charged. However, according to the literature, the gas flow rate entering the ANG vessel is usually considered fixed to the best of the author's knowledge, and a flow controller with a respecified set point was used in the experiments [17, 23-26]. Besides, due to the pressure drop and gas expansion during the charging, when high-pressure gas is injected into an empty tank, a relatively significant temperature drop in the inlet gas is expected (especially in a short-initial time of complete charging) [27]. The inlet gas temperature variation is also neglected in the studies, and the inlet temperature is considered a fixed value [22, 25, 26, 28].

Here in this research, we collected experimental data for dynamic adsorbed methane storage using our in-house custom-built ANG vessel. Two different types of homemade coal-based adsorbents with a high methane storage capacity of ≥175 ($cm^3_{(STP)}/cm^3$) were fabricated, characterised and used to investigate the thermal fluctuations inside the ANG vessel during dynamic CH_4 injection. The collected data was used for validation of our simulated charge endeavour's corresponding process. In the simulation, the incorrect assumptions of constant gas flow rate and temperature during charging of ANG capsules, which are usually adopted in the existing research corresponded to the ANG technique, were waved. Thus, the inlet gas flow rate and temperature were allowed to vary with time in all the simulations to mimic the actual charging process and the effect of variable flow rate during the charging process on the ANG vessel's overall performance was investigated. Besides, the adiabatic expansion effect and the resulting temperature drop of high-pressure gas

after injection into the ANG bed was systematically analysed using Aspen HYSYS Process Simulation Software. Finally, the ANG storage compartment's thermal behaviour was successfully modelled by a set of 2D partial differential formulations which were solved numerically using the COMSOL Multiphysics software.

2. Theoretical background

Modelling strategies are usually based on formulating mass and energy balances for the desired system, with a greater or lower degree of sophistication in the process's physical description. The present section's primary intention is to develop a numerical model that provides necessary details for studying and evaluating an ANG system's performance during the charging condition.

2.1 Mathematical modelling of the ANG vessel

Herein, a two-dimensional axisymmetric mathematical model was used to develop the ANG system's transient heat and mass transfer analysis during the single component charging. The output variables of the storage vessel model, T (r, z, t) and P (r, z, t), are obtained from the simultaneous solution of the differential mass and energy balance equations, subject to the appropriate boundary and initial conditions imposed to the adsorbent bed. The ANG system comprises a portable cylindrical vessel with a length of L and inside diameter of D_i, filled with a homogeneous medium of adsorbent powder (i.e. AC1 or AC2). The small opening diameter of D_f, located in the ANG cylinder's front face, provided the entranceway of gas flow during charging and withdrawal (see Figure 1).

The following assumptions are made in the analysis to simplify the proposed model:

(i) The 2D-axisymmetric model is studied; the parameters' variations are considered only in radial and axial directions through adsorbent bed [22, 26, 29].

(ii) The adsorbent particles are uniform in size and packed inside the ANG cell with constant bed porosity [12, 25, 28]. The specific heat and density of the dry adsorbent are constant over the whole operating conditions.

(iii) Intra-particle and film resistances to mass and heat transfer are neglected [12, 25, 28]. Thus, no distinct mass and energy balances for the non-adsorbed flowing phase and the adsorbent was applied.

(iv) Methane is considered as an ideal gas because for the *P-T* ranges of study (0-35 bar, 283-363 K), the average value of the methane compressibility factor is 0.97 [25, 28, 30].

(v) The thermo-physical properties of the adsorbent materials (density, specific heat capacity, thermal conductivity) are assumed to be constant [28, 29].

(vi) The isosteric heat of methane adsorption on each adsorbent was considered constant [25, 26, 28].

(vii) Thermophysical properties of steel, together with viscosity and specific heat of methane, are assumed to be constant over the operating range of pressure and temperature [25, 26, 28, 31].

The basic structure of our proposed model is founded on transport phenomena relations wherein mass, momentum and energy balance equations happen inside the porous media [25, 26, 28]. Additionally, the Dubinin-Astakhov (DA) isotherm model was recruited to calculate the equilibrium adsorption capacity dynamically. Further description of the model was presented as follows:

Continuity equation

$$\frac{\partial}{\partial t}\left(\varepsilon_t.\rho_g+\rho_b.q\right)+\frac{1}{r}\frac{\partial}{\partial r}\left(\rho_g.r.v_r\right)+\frac{\partial}{\partial z}\left(\rho_g.v_z\right)=0 \quad (1)$$

Wherein ε_t is total porosity, ρ_g is gas density (kg/m^3), ρ_b is bed density (kg/m^3), q is gravimetric amount of adsorbed gas (kg/kg), r is radial coordinate, v_r is velocity at radial direction (m/s) and v_z is velocity at axial direction (m/s). Equation (1) illustrates the continuity equation (mass balance) in both phases of the gaseous ($\rho_g = PM_{\mathrm{CH4}}/RT$) and adsorbed ($\rho_b$) for the single component charging process [14, 19, 25].

$$\varepsilon_t=\varepsilon_b+(1-\varepsilon_b)\times\varepsilon_p\ ,\ \varepsilon_p=\frac{V_t\times\rho_p}{1-\varepsilon_b} \quad (2)$$

Equation (2) represents the total porosity of the adsorbent bed (ε_t) has contributions from micropores, mesopores, macropores (ε_p) and interparticle void spaces of adsorbent structure which is also known as the bed porosity (ε_b) [22, 26, 32]. The average value of 0.35 for either of the adsorbents' bed porosity was assumed based on the experimental data reported in references [18, 21, 32]. To calculate the particle porosity (ε_p), two terms of the total pore volume of the adsorbents

(V_t), particle density of powder AC (ρ_p) are needed. More information about these parameters has been declared in Supporting Information (SI), still, the corresponded values are listed in Table 1.

Momentum equation

Navier Stokes equations for homogeneous gas flow in two dimensions of r and z inside the porous medium are given as [19, 24, 25]:

r-momentum equation

$$\frac{\rho_g}{\varepsilon_t}\left(\frac{\partial v_r}{\partial t}\right)+\frac{\rho_g}{\varepsilon_t^2}\left(v_r\frac{\partial v_r}{\partial r}+v_z\frac{\partial v_z}{\partial z}\right)=-\frac{\partial P}{\partial r}-\frac{\mu_g}{K}v_r+\mu_g\left[\frac{1}{r}\frac{\partial}{\partial r}\left(r\frac{\partial v_r}{\partial r}\right)+\left(\frac{\partial^2 v_r}{\partial z^2}\right)\right] \quad (3)$$

z-momentum equation

$$\frac{\rho_g}{\varepsilon_t}\left(\frac{\partial v_z}{\partial t}\right)+\frac{\rho_g}{\varepsilon_t^2}\left(v_r\frac{\partial v_r}{\partial r}+v_z\frac{\partial v_z}{\partial z}\right)=-\frac{\partial P}{\partial z}-\frac{\mu_g}{K}v_z+\rho_g.g+\mu_g\left[\frac{1}{r}\frac{\partial}{\partial r}\left(r\frac{\partial v_z}{\partial r}\right)+\left(\frac{\partial^2 v_z}{\partial z^2}\right)\right] \quad (4)$$

Wherein μ_g is gas viscosity (kg/m.s), g is gravity (m/s^2) and K is permeability of the bed (m^2).

Energy equation

The two-dimensional transient axisymmetric energy equation was used to monitor the temperature variation through the absorbent bed [18, 19, 22].

$$(\rho C_p)_{eff}\left(\frac{\partial T}{\partial t}\right)+(\rho C_p)_g\left(v_r\frac{\partial T}{\partial r}+v_z\frac{\partial T}{\partial z}\right)=\frac{1}{r}\frac{\partial}{\partial r}\left(\lambda_{eff}\frac{\partial T}{\partial r}\right)-\lambda_{eff}\frac{\partial^2 T}{\partial z^2}+(\rho_b.\Delta H_{ads})\frac{\partial q}{\partial t} \quad (5)$$

Wherein C_p is the specific heat capacity at constant pressure (J/kg.K) and ΔH_{ads} is isosteric heat of adsorption (J/mol). The effective heat capacity $(\rho C_p)_{eff}$ and the effective thermal conductivity (λ_{eff}) for a homogeneous mixture of the adsorbent is given by the following expressions [18, 22].

$$(\rho C_p)_{eff}=\left(\varepsilon_t.\rho_g+\rho_s.q\right)C_{pg}+(1-\varepsilon_t)\rho_s.C_{ps} \quad (6)$$

$$\rho_b=(1-\varepsilon_t)\rho_s\ ,\quad \lambda_{eff}=\varepsilon_t.\lambda_g+(1-\varepsilon_t)\lambda_s \quad (7)$$

In these equations, ρ_s is solid density (kg/m^3), C_{ps} and C_{pg} are respectively the specific heat capacity at solid and gas phase (J/kg.K), λ_g and λ_s are thermal conductivity (W/m.K) at gas and solid phase separately.

2.2 Adsorption isotherms

The adsorption isotherms data are crucial in the design of the ANG storage system. The quantity of gas adsorbed per unit mass of adsorbent is defined as concentration, synonymous with loading or uptake. The equilibrium gravimetric methane uptakes (q) on either of the adsorbents were measured via our custom-built volumetric gas adsorption apparatus. We have described this sorption measurement system's details, calibration method, and measurement procedure in our previous studies [33, 34] and briefly in the Supplementary Information. Moreover, the volumetric methane adsorption isotherms for the AC1 and AC2 were depicted in Figure S3 and the values tabulated in Tables S2 and S3. These experimental data have been regressed using the Dubinin-Astakhov isotherm model; the values of the fitted model fitted parameters were reported in Table 1. Unlike some of the well-known isotherm models, DA isotherm considers surface heterogeneity, and it is capable of good fitting over a high range of pressure and temperature [12, 20, 24]. The amount of adsorbed gas (q) inside the ANG cell is calculated by the following equations.

$$q=\rho_{ads} W_0 \, exp\,[-(A/\beta.E_0)^n] \qquad (8)$$

$$\rho_{ads}=\frac{\bar{\rho}_{ads}}{exp[\alpha_e(T-T_B)]}\ ,\ A=RTln\left(\frac{P_s}{P}\right)\ ,\ P_s=P_{cr}\left(\frac{T}{T_{cr}}\right)^2 \qquad (9)$$

In these equations, ρ_{ads} is adsorbed density (kg/m^3), W_0 is maximum volumetric adsorbate uptake of the adsorbent (m^3/kg), A is Polony's adsorption potential, β is affinity coefficient, E_0 is activation energy (J/mol), n is DA exponent, $\bar{\rho}_{ads}$ is the density of liquid methane at the normal boiling point (kg/m^3), α is thermal expansion coefficient (1/K), T_B is temperature boiling (K), R is the universal gas constant (J/mol.K), P_s is saturation vapour pressure (bar), P_{cr} is critical pressure, and T_{cr} is the critical temperature (K).

2.3 Initial values and boundary conditions

As mentioned earlier, COMSOL Multiphysics was used to solve the coupled partial differential equations (PDEs). The software runs the finite element analysis together with adaptive meshing and error control using a variety of numerical solvers. A more detailed description of this mathematical and numerical foundation appears in the COMSOL Multiphysics User's Guide and the COMSOL Multiphysics Modeling Guide [35].

Initially at t=0, the storage vessel is at ambient pressure (P_i) and initial bed temperature (T_i), and q is equal to $q_{eq}(P_i,T_i)$. COMSOL Multiphysics software requires time variations of the entering gas flow rate during the charging process to successfully simulate the entire storage process for the previously user-defined mathematical models. Therefore, at the opening, boundary (2), for the inlet gas, the following boundary condition was applied:

$$\text{For} \quad z=0,\ 0 \le r \le R_i\ ,\ t>0 \qquad v_{inlet}= Q_{ANG}/A_{inlet}\ ,\ T=T_{inlet} \tag{11}$$

Where v_{inlet} can be obtained by dividing the gas flow rate (Q_{ANG}) at the charging condition by the cross-sectional area of the inlet (A_{inlet}). The inlet temperature profile (T_{inlet}) was obtained from a time-dependent equation developed according to the collected experimental data; this equation and its derivation approach were discussed in section 3.3. From the thermodynamic point of view, the entering gas experiences an adiabatic expansion that results in a drastic temperature drop, results in changes in the entering gas flow rate [27]. In this work, it was not operationally possible to install a temperature sensor right at the entering zone to monitor the temperature drops. However, we used powerful HYSYS Software V.11 to systematically analyse the temperature variation right after the gas entered during the charging condition. More information about this topic was precisely discussed in section 3.3.2.

As depicted in Figure 1(A), along the longitudinal axis (boundary 1), the symmetry condition can be written as follow:

$$\text{for}\ \ 0\le z\le L\ ,\ r= 0,\ \ t>0,\ \ \frac{\partial T}{\partial r}=0 \tag{12}$$

Also, the no-slip boundary condition ($v_g=0$) is applied on all rigid walls, boundaries 3-6, depicted in Figure 1(A). The heat source at the inlet boundary (2) is given as:

$$\dot{Q}_{BHS}=-\acute{n}.(\lambda_{eff}\nabla T)=\left(\rho C_p\right)_g v_{inlet}(T_s-T) \tag{13}$$

Where n' is unit outward normal to the surface and T_s is the solid's temperature (K).

The convective heat transfer boundary conditions are imposed for walls numbered 3-6.

$$\dot{Q}_{conv}=-\acute{n}.(\lambda_{eff}\nabla T)= h_c(T_{amb}-T) \tag{14}$$

Where h_c is convective heat transfer coefficient (W/m^2.K) and T_{amb} is the ambient temperature (K).

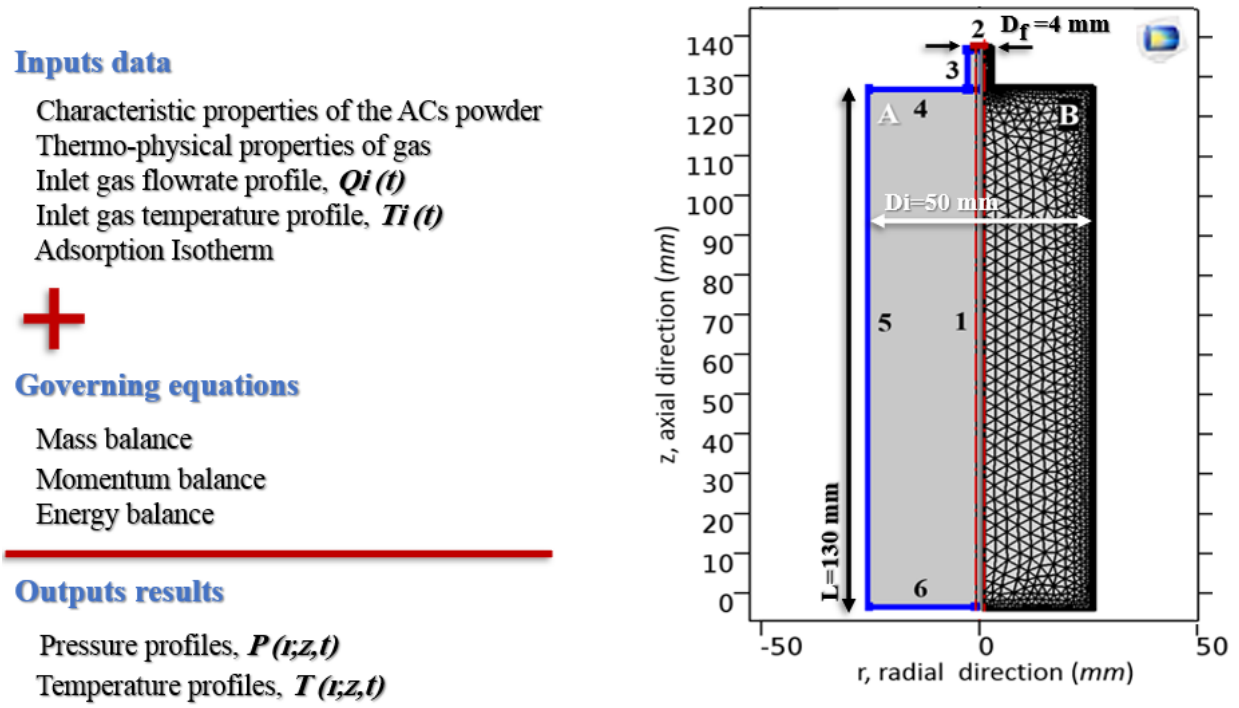

Figure 1. *Schematic diagram of the ANG storage system accompanied by input-output data. (A) Defined boundaries of the 2D axisymmetric model used for ANG system simulation. (B) Typical finite element mesh generated over ANG simulation domain.*

2.4 Solving the mathematical model via COMSOL Multiphysics

The mathematical modelling for the ANG storage system, which includes the governing equations, adsorption isotherm model and the boundary conditions (equations (1)-(14)), were numerically solved using COMSOL Multiphysics 5.3*a* software. The discretisation domain in an axially symmetric r-z coordinate system was conducted based on the finite element method. First, simulation domains meshed with different sizes (i.e. normal, fine, finer and extra fine). Then, to verify the simulation results, the proper mesh sizing across the numerical calculation will be selected (section 4.2). As discussed later, all simulations have been carried out using a finer unstructured grid (triangular elements) mesh with a maximum element size of 0.875 mm, minimum element size of 0.025 mm, and maximum element growth rate of 1.13 mm. For

visualisation purposes, a typical coarse mesh is shown in Figure 1 (B). Based on an absolute error at the mesh points, a convergence criterion has been set equal to 10^{-6}.

The thermophysical properties of methane and the relevant input data used in the simulation are shown in Table 1. Furthermore, the characteristic properties of adsorbents AC1 and AC2 as input data for the simulation validation have been reported in Table 1, separately.

Table 1. Thermophysical properties of methane and the adsorbents characteristic data used in the simulations.

Methane			Adsorbents			
Input data	*Value*	*Reference*	*Input data*	*Value* *AC1*	*AC2*	*Reference*
M_g (kg/mol)	16.04×10^{-3}	[36]	ρ_b (g/cm^3)	0.50	0.73	This work
$(C_p)_g$(J/kg.K)	2450	[30]	ρ_p (g/cm^3)	0.39	0.49	This work
R (kJ/mol K)	8.314	[25]	ρ_s (g/cm^3)	1.90	1.90	This work
λ_g (W/m.K)	0.0343	[29]	$(C_p)_s$(J/kg.K)	900	740	[22] & [37]
μ_g (kg/m.s)	1.25×10^{-5}	[18]	λ_s (W/m.K)	0.54	0.54	[22]
P_c (bar)	45.99	[36]	ε_t	0.86	0.92	This work
T_c (K)	190.56	[36]	n	1.33	1.84	This work
T_B(K)	111.67	[36]	E_0 (J/mol)	5261.1	5842.6	This work
ρ_{ads} (g/cm^3)	0.42	[36]	V_t (cm^3/g)	0.84	0.74	This work
β	0.35	[38]	T_i (K)	282.5	289	This work
h_c (W/m^2.K)	5	[22]	T_{amb} (K)	282.5	289	This work
α_e (1/K)	0.0025	[22, 26]	ΔH_{ads} (J/mol)	19400	24650	[28] & This work

3. Experimental

This section presents a brief overview of the equipment and experimental technique for data collection during the charging process.

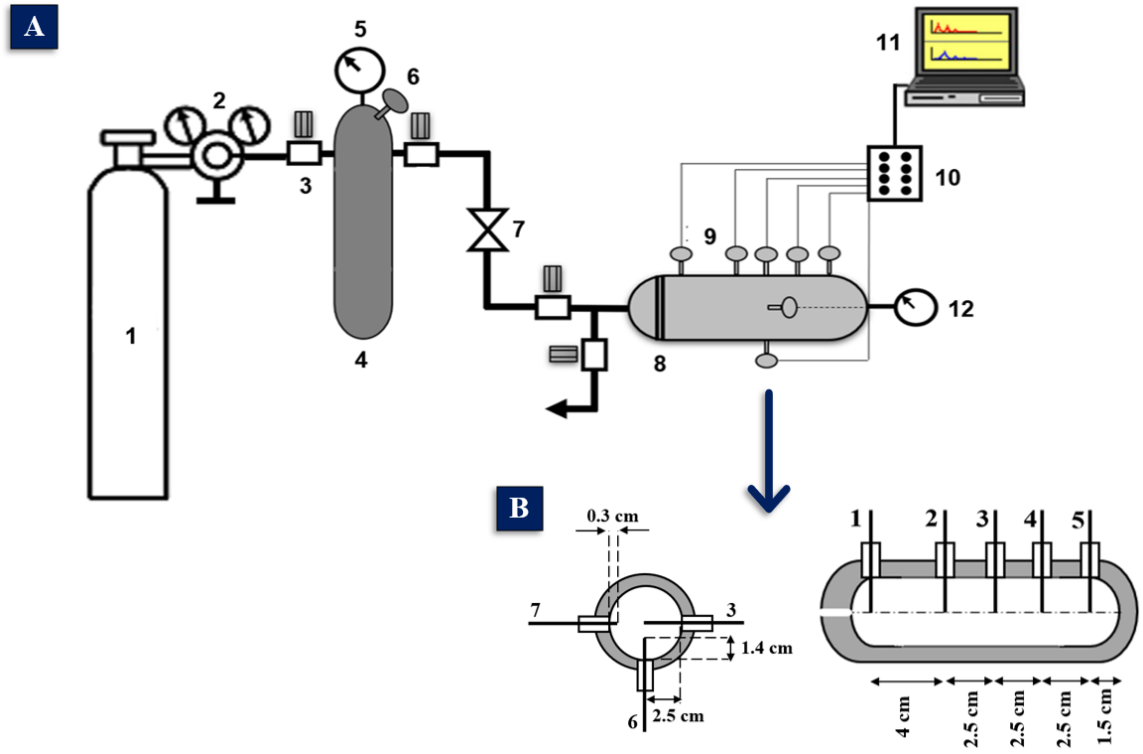

Figure 2. *(A) A schematic diagram of the experimental setup (1) gas cylinder, (2) pressure regulator, (3) valves, (4) doser, (5) pressure gauge, (6) PT 100 temperature sensor; (7) metering valve; (8) ANG storage vessel; (9) PT 100 temperature sensors; (10) temperature data logger; (11) computer; (12) pressure gauge. (B) Arrangement of seven custom-built temperature sensors inside the ANG vessel.*

3.1 ANG setup description

The experimental apparatus was constructed in our laboratory to study the performance of various ANG system elements. As shown in Figure 2 (A), the testing apparatus consists of a high-pressure reference vessel (usually referred to as "doser") with a volume of 1000 cm^3 to control the amount of methane injection to the ANG cell (adsorption vessel). The ANG cell is a high-pressure stainless-steel cylindrical vessel with an internal cylinder length of 130 ± 0.1 mm and an inside diameter of 50 ± 0.1 mm. The vessel's wall thickness is 25 ± 0.05 mm, and the corresponding top and bottom caps thicknesses are 30 ± 0.05 mm and 25 ± 0.05 mm, respectively. The cell's internal volume is 292 ± 0.05 cm^3. The vessel has a small opening in the top cap centre with a 4 ± 0.03 mm diameter used to charge and discharge the cell. Both doser and ANG vessels were made under

ASME code recommendations (ASTM A-516/A516M-17 steel) and tested at 100 bar pressure for several days [39].

As schematically depicted in Figure 2(B), the ANG storage vessel is equipped with seven PT100 temperature sensors (with an accuracy of ±0.1 °C). The sensors are distributed through the vessel as follows: two sensors are placed at the midst of cylinder with the radial spacing of 11 ± 0.5 mm, four sensors are located along the cylinder axis with the axial spacing of 25 ± 0.1 mm, and the last sensor measures the inlet gas temperature before entering the adsorption bed. Two portable pressure indicators (MN18/L nuovafima, with the accuracy of 0.1% FS) were used to monitor the doser and ANG vessel's working pressure. A metering valve (valve number 7) was placed between the doser and the ANG vessel to provide accurate gas flow rate control entering the ANG vessel. During all tests, the metering valve was set at the 50% opening position.

3.2 Materials

Two different types of powder coal-based activated carbons (AC1 and AC2), fabricated and characterised in our previous works for ANG application [33, 34], were used as the adsorbents in the ANG vessel. Summary of the preparation condition, porous structural properties and CH_4 storage/delivery capacity of the adsorbents are reported in Table 2. Ultra-high purity methane of 99.999%, provided by Technical Gas Services, UAE, is used as the adsorbate.

Table 2. Characteristics properties of the in-house fabricated adsorbents used in our ANG setup.

Adsorbent	*Precursor*	*Thermal Condition*		S_{BET} (m^2/g)	V_{tot} (cm^3/g)	ρ_{pack}^{*} (g/cm^3)	CH_4 *uptake*** $(V_{(STP)}/V)$	CH_4 *delivery**** $(V_{(STP)}/V)$
		Carbonisation	Activation					
AC1	Anthracite	-	1003 K for 1h	2160	1.12	0.53±0.03	175	100
AC2	Coal tar pitch	873 K for 3h	1073 K for 3h	2261	1.23	0.70±0.03	184	110

*Packing density or bulk density calculated by pressing the powder to 500 kg/cm^2 [40].
** Measured at 40 bar pressure and 298 K. Calculation method was described in Supporting Information (see Eq (S1)).
*** Obtained by the difference of methane adsorbed between 35 and 5 bar at 298 K. Graphical calculation method was depicted in Figure (S3).

3.3 Experimental procedure

About 200 g of the ACs were degassed in an oven at 383 K overnight before each experiment. The adsorbents were manually packed inside the ANG vessel, and then the cap was closed and sealed

carefully. The doser was filled with methane by opening the high-pressure valve (3), up to 40-45 bar pressure. Dynamic charge tests were conducted by fully opening the high-pressure valves of (a) and (b) (Figure 3). The charging was deliberately terminated when the pressure of the ANG vessel reached 40 bar. The variations in the cell's temperature were carefully recorded during each charging experiment.

3.3.1 Measurement of the inlet gas flow rate

A reliable volumetric approach was applied to estimate the flow rate of inlet gas to the ANG vessel at any time during the charging process. This was done by resorting to the flow resistance concept in a constant restriction. The restriction was included both fully opened gate valves of (a) and (b) and half-opened metering valve (7), as schematically depicted in Figure 3. At the start of each experiment, valves (7) and (b) were kept half and fully opened, respectively, and valve (a) was fully closed. Then the doser was filled with methane up to a certain pressure of about 40 - 45 bar. Afterwards, valve (a) was opened to initiate the charging of an empty tank (with no adsorbents) similar to a compact natural gas (CNG[1]) tank. After opening valve (a) at t=0, the history of various parameters (P_d, T_d, P_{CNG} & T_{CNG}) were accurately recorded at different time intervals. The laboratory environment ($P_b \cong 1.014$ bar) was used to calculate the absolute pressures in both doser and CNG vessels from their corresponding gauge readings. Peng–Robinson equation of state [41] was used to compute methane molar contents of both CNG and doser (d) vessels at any desired time (equations (15) to (17)).

$$N_i = (P_i V_i)/(Z_i R T_i) \qquad \text{where } i = CNG \text{ or } d \tag{15}$$

$$\Delta N_i = \int_0^t N_i dt = \int_{P_0}^{P_t} \frac{V_i dP_i}{Z_i R T_i} \tag{16}$$

In these equations, ΔN, ΔP, V, Z, R, T respectively denotes the molar flow at a specific time interval of t, the pressure change in the vessel from the initial state (P_0) to the final pressure after a specific time (P_t), vessel's volume, gas compressibility factor, the universal gas constant and vessel's temperature. It should be noted that subscripts of "d" and "CNG" indicate the corresponding parameters of doser and CNG vessels. According to Table 3, the pressure difference between two

[1] CNG vessel is an ANG vessel in the absence of adsorbent.

specific time intervals in doser and CNG vessels result in estimating ΔN_d and ΔN_{CNG} respectively. From the theoretical point of view, the molar flow that leaves the doser (ΔN_d) at a specific time interval must be equal to those that enter the CNG vessel (ΔN_{CNG}). However, these two parameters' obtained values were not the same at any desired step (see Table 3). The reasonable explanation for such differences might be related to the fact that all experimental measurements have some degree of uncertainty that originated from random or systematic errors. To reduce these unwanted errors in mole content calculation, we used averaging molar flow (ΔN_{ave}) over ΔN_d and ΔN_{CNG} according to equation (17).

$$\Delta N_{ave} = (\Delta N_d + \Delta N_{CNG})/2 \quad (17)$$

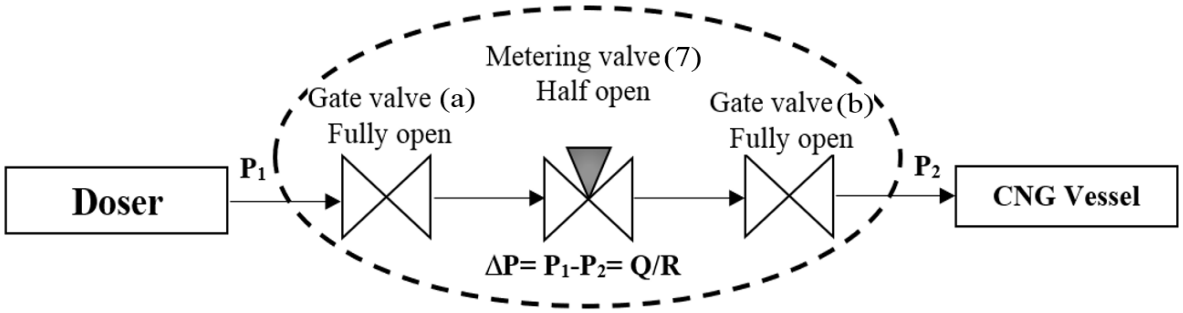

Figure 3. *Schematic representation of flow resistance of the entire valve system between doser and CNG vessel.*

Table 3 provides the experimental results obtained to find an overall resistance (*R*) for the entire valving system. Figure 4 illustrates the computed valving system resistance (R) variations versus the doser and CNG tanks' corresponding pressure difference. The fitted line was used in all ANG experiments to predict the gas's initial flow rate entering the CNG capsule.

Table 3. Experimental readings and calculation results during pressure changes in doser and CNG cells.

time (s)	P_d (bar)	T_d (K)	ΔN_d (mol/s)	P_{CNG} (bar)	T_{CNG} (K)	ΔN_{CNG} (gmol/s)	ΔN_{ave} (gmol/s)	$\Delta P = P_d - P_{CNG}$	$R = \Delta P/\Delta N_{ave}$
0	42.5	290	0.055	0	290	0.045	0.0500	42.5	935.429
2	40	290	0.061	7	288	0.047	0.0540	33	694.737
4	37.5	289	0.039	14	282	0.032	0.0350	23.5	731.815
7	35	289	0.024	21	287	0.029	0.0260	14	481.188
12	32.5	289	-	31	287	-	-	-	-

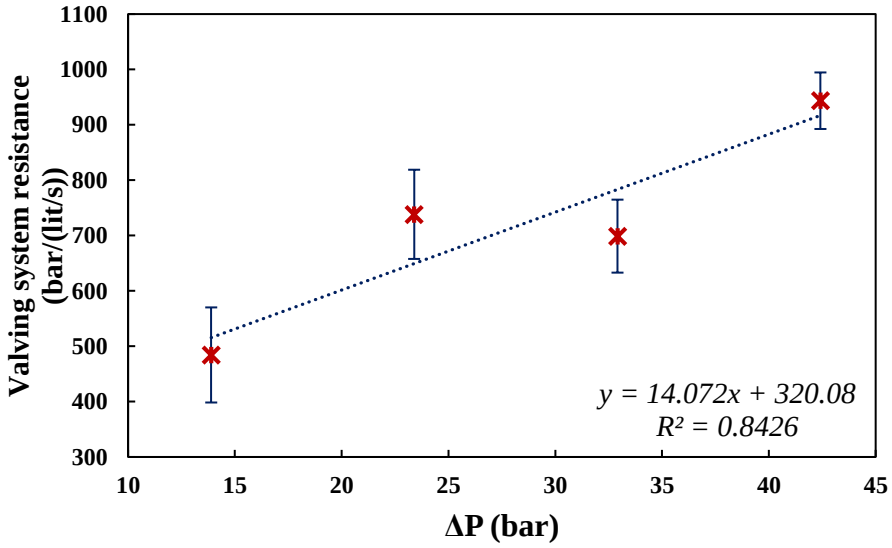

Figure 4. *Variations of valving system resistance with the corresponding pressure difference between doser and CNG tank.*

3.3.2 Boundary conditions data collection and pre-processing for ANG charging process

After packing the ANG tank with each of the adsorbents, a data set was collected to assess the current modelling and corresponding simulation's performance. Table 4 provides the dynamic pressure variations of both doser and packed ANG vessels during the charging process. The estimated mole differences (ΔNs) between the vessels were used to find the inlet gas flow rate (L/s)

entering the ANG tank. Aspen HYSYS Process Simulation Software V.11 was employed to predict the ANG temperature drop across the valving system (due to adiabatic expansion) and the corresponding compressibility factor. The Peng–Robinson equation of state was considered as a property package for this simulation study. Figure 5 illustrates the fitted trends and the corresponding equations for inlet temperature and the actual volumetric flow rate. These equations are used in COMSOL Multiphysics software to predict the inlet boundary condition at any desired instance.

Table 4. Dynamic pressure variations and calculation results during pressure changes in both doser and ANG cell packed with different adsorbents of AC1 and AC2.

Time (s)	P_d (bar)	P_{ANG} (bar)	$\Delta P = P_d - P_{ANG}$	R^* (bar/(mole/s))	$\Delta N = \Delta P/R$ (gmole/s)	$T_{ANG,in}$ (K)	Q_{ANG} (L/s)
				AC1			
0	55	0	55	1084.060	0.051	256.4	1.084
39	50	9.5	40.5	881.727	0.046	264.6	0.103
111	47.5	18	29.5	728.233	0.040	271	0.048
134	45	23	22	623.578	0.035	275.2	0.031
153	42.5	30	12.0	491.015	0.025	280.2	0.018
170	40	39	1	330.544	0.003	286	0.002
				AC2			
0	55	0	55	1084.060	0.051	257.8	1.089
43	51.5	9	42.5	909.635	0.047	264.8	0.112
116	48.75	17.75	31	749.164	0.042	271.4	0.051
139	45.5	24	21.5	616.601	0.035	276.6	0.032
157	43	29.50	13.5	504.969	0.027	280.8	0.019
175	40	39	1	330.544	0.003	287.1	0.002

*Calculated from the fitted equation presented in Figure 4.

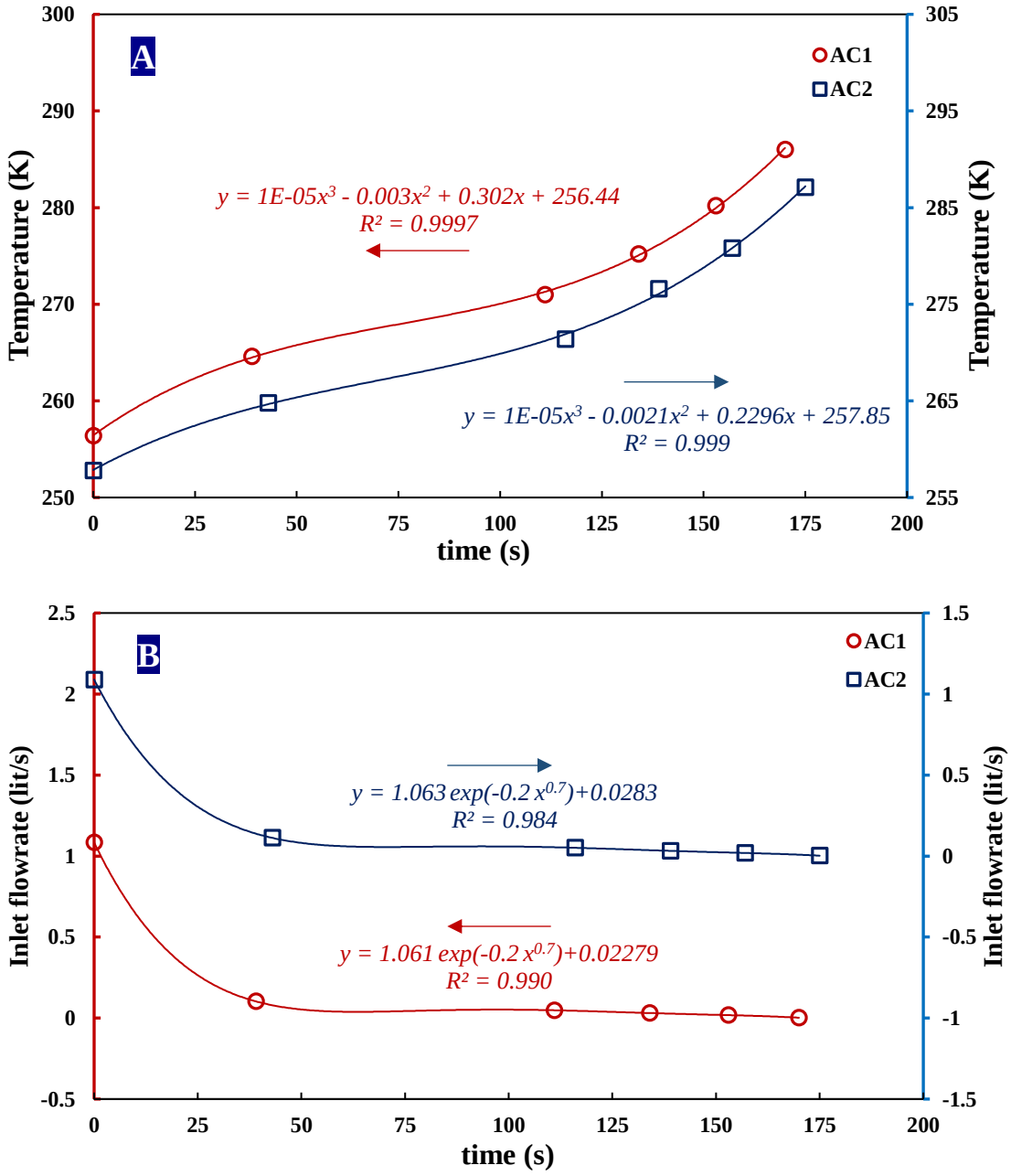

Figure 5. *Fitted profiles for (A) inlet temperature and (B) corresponding flow rates used as the dynamic boundary conditions in COMSOL software.*

4. Results and Discussion

The experimental records of pressure and temperature inside the ANG vessel during continuous charging were first described and discussed in this section. Afterwards, the distributed mathematical model's simulation results were validated with the data obtained from the experimental charging process.

4.1 ANG charging process data collection

After filling the doser, methane was charged into the prototype ANG vessel packed with regenerated adsorbents of AC1 or AC2, according to the experimental procedure described in section 3.3. The pressure profiles inside the bed were measured during the charging, and the results are illustrated in Figure 6. The results confirm a pressure enhancement inside the vessel during the charging, resulting from the accumulation of gas molecules in the void spaces between the solid particles. During the continuous gas loading, depending on the inter and intra-particle mass transfer resistance inside the bed and the rate of gas adsorption, part of the gas molecules will be adsorbed, and the balance remains in the bed's empty spaces. The pressure rise in the tank is expected to increase faster after the saturation of the adsorbents when no further adsorption occurs inside the tank [41].

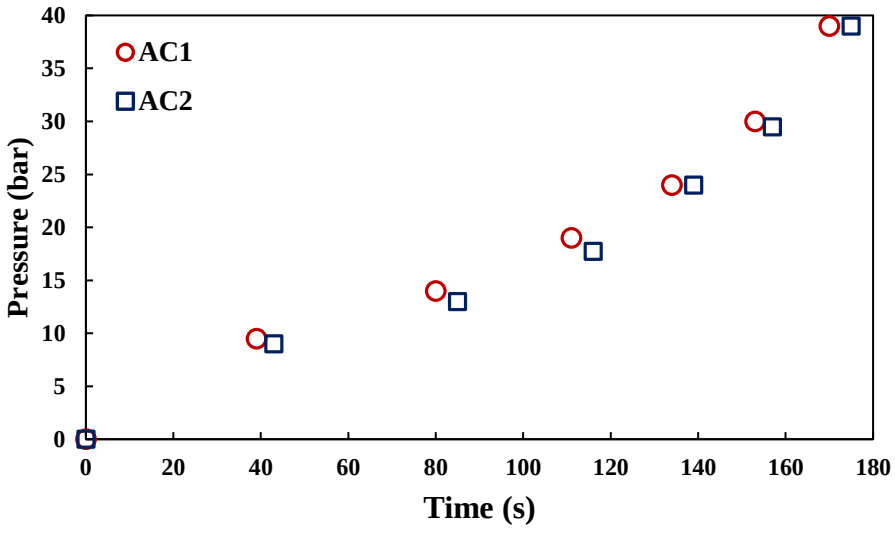

Figure 6. *Pressure profiles for AC1 and AC2 during the charging process.*

Figure 7 provides part of the collected temperature data at eight different points of the ANG bed (Figure 2(B)) during the charging process. The corresponding temperature values are also reported in Tables S4 and S5 of the SI. These temperature profiles later were used for validation of the simulation results. The bed temperature variations in points 1 to 7 for both adsorbents follow a similar trend, showing an ascending path consisting of two regions before and after 20 seconds.
In the first 20 seconds of gas loading, "*Region I*" of the tank's temperature profile graph (Figure 7), a significant temperature rise was observed in a short duration resulting from the heat of adsorption after introducing the gas to regenerated solids [10]. The width of this zone depends on the porosity and surface chemistry of the adsorbent. In other words, adsorbent characteristics play a significant role in temperature enhancement, especially in the *Region I*, where the adsorption process happens quickly. This region holds useful information regarding the initial temperature distribution and storage start-up heating function [17]. After 20 seconds, in *Region II*, the temperature gradient increase becomes slower. The main reasons for the lower slope than the first region are saturation of adsorption sites and heat transfer flux from the ANG tank's walls to the surrounding environment [12, 17]. The second region helps to understand the maximum temperature in the tank and its influence on storage efficiency during charging.

During the gas loading, the ANG bed's centre filled with AC1 was heated up to 322.1 K and 319.8 K at sensors 3 and 2, net rises of 33 K and 31 K, respectively. In the same adsorbent system, sensors 1 and 5, located at the inlet and bottom of the ANG chamber, show a temperature rise to 303.1 K and 304.1 K, equivalent to a net increase in temperature 20.1 K and 21.1 K, respectively. Similarly, the maximum temperature rise in the AC2 bed was at the central sensors of 2 and 3, where the temperature reached 322.1 K and 319.8 K, respectively (with a net increase of 33.1 K and 30.5 K). Moreover, the lowest sensed temperature values in the absorption chamber were related to sensors 1 and 7, with a temperature variation of 315.9 K and 316.9 K, respectively.

Table 5 reports the average temperature values of the bed as well as the axial and radial directions during the charging process. Temperature enhancement in the AC2 bed is higher than those recorded for the ANG tank filled with AC1. The high-temperature values reported for the AC2 bed can be explained by the higher methane uptake capacity of AC2 (184 $cm^3_{(STP)}/cm^3$) in comparison with that of AC1 (175 $cm^3_{(STP)}/cm^3$).

Table5. Average ANG bed temperatures during methane loading.

Adsorbent	*Time*(s)	*Average bed Temperature* (K)	*Average axial Temperature* (K)	*Average radial Temperature* (K)
AC1	170	317.69	323.67	322.41
AC2	175	331.00	338.10	337.26

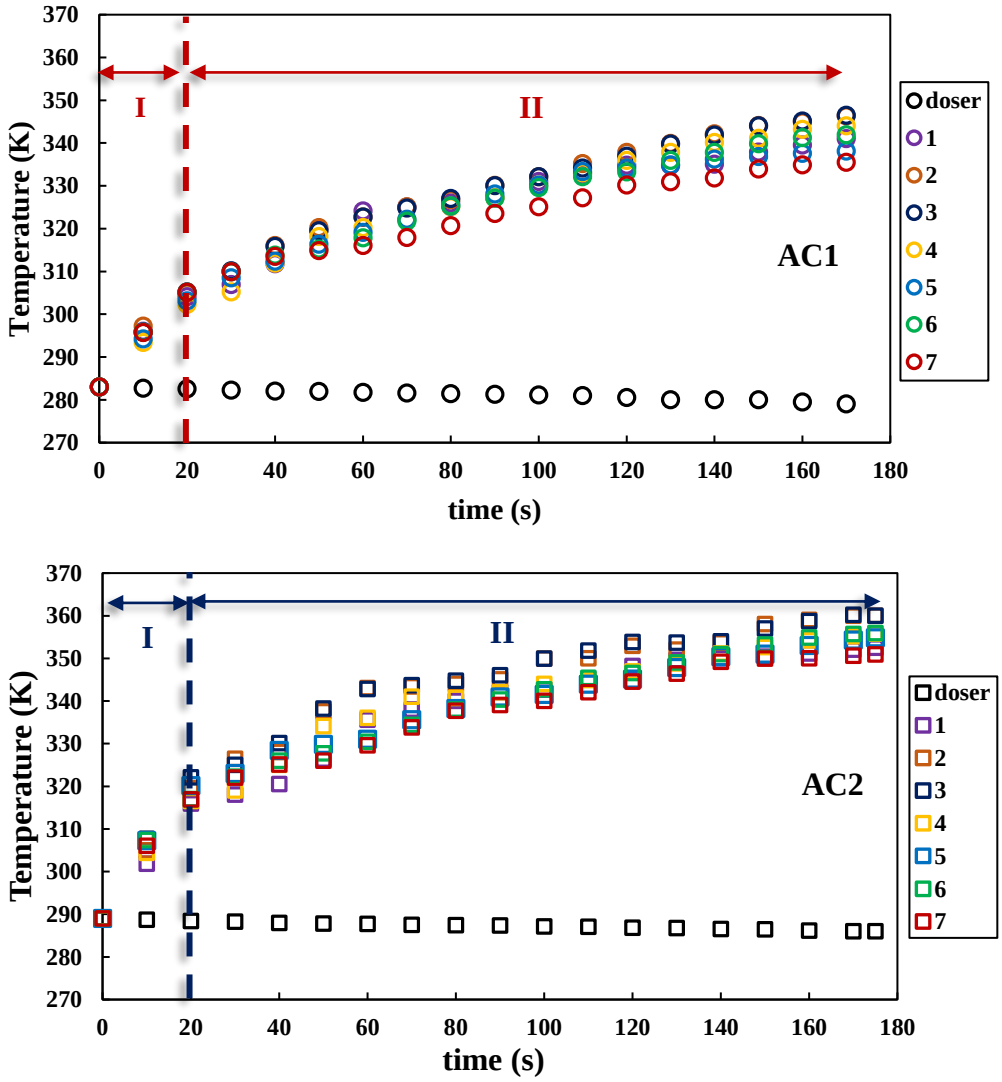

Figure 7. *Measured temperature profiles for both doser and ANG vessel during the charging process using two various adsorbents of AC1 and AC2.*

From a practical point of view, the entire ANG vessel warms up during charging. However, at the ANG vessel entrance, a temperature drop is expected because of the adiabatic expansion of

compressed methane [17, 25]. The low temperature of the inlet gas disappears immediately with further gas loading and pressurising the bed. In the present study, the temperature variation of the inlet gas was not experimentally measured at the entering point; however, this cold region's effect is visible on the temperature profiles of sensor 1 (nearest sensor to the gas entrance zone) for both absorber systems.

4.2 Simulation results of ANG system during the charging process

The simulation results of the ANG vessel's pressure and temperature profiles are separately presented in Figures 8 and 9. As shown in Figure 8, continuous methane loading makes the pressure contour curves inside the tank predict the rising trend during the charging process. Over higher loading times, a uniform pressure distribution was achieved throughout the ANG bed. This result proves the adsorbent bed's high permeability, which allows the gas to transfer all over the bed freely (i.e. AC1 and AC2) [12].

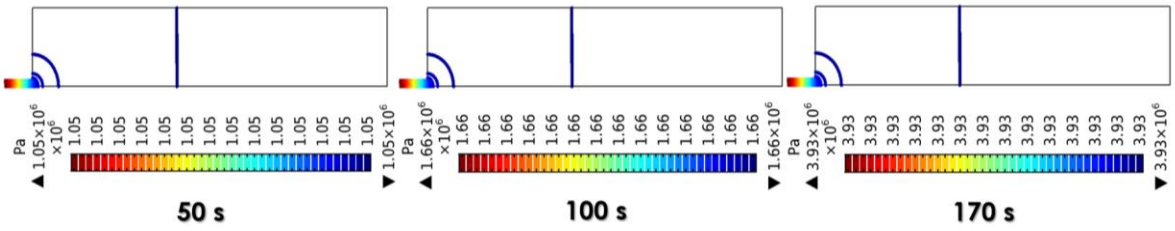

Figure 8. *Pressure contours inside ANG vessel (filled with AC1 adsorbent) for different times of 50, 100 and 170 s of the charging process.*

As the adsorption process begins, the adsorbent bed's temperature increases due to the release of adsorption heat. The ANG bed suffers from further adsorption heat due to the low heat transfer rate from the bed to the surrounding environment by elapsing the loading time. The heat generated inside the adsorption chamber affects the central points more than the other sections. All the results mentioned above are presented in 2D and 3D temperature profiles of Figure 9.

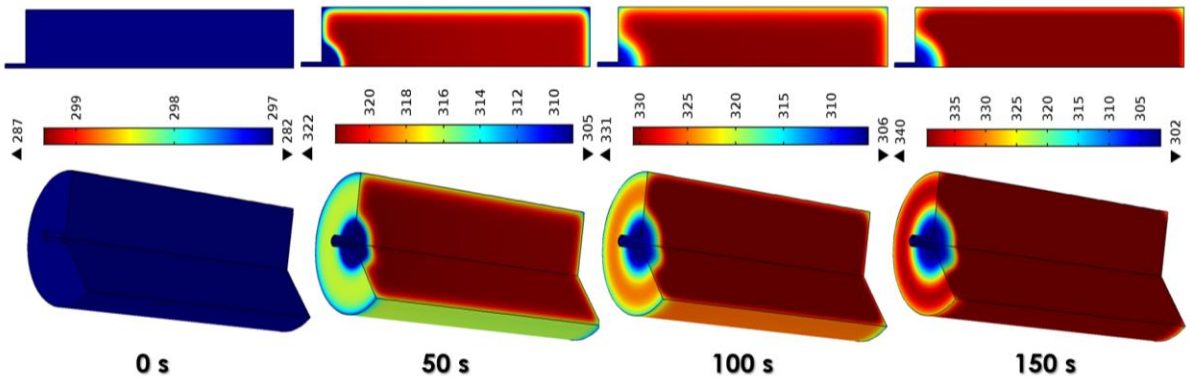

Figure 9. *2D and 3D temperature profiles inside the ANG vessel (filled with AC1) initially (0 s) and at different gas loading times of 50, 100 and 150 s.*

Figure 10 compares the simulation results and the experimental data for the pressure variations inside the ANG bed during the charging operation. The solution domain was discretised by different sizes (i.e. normal, fine, finer and extra fine) to select a proper mesh sizing across the numerical calculations. The numerical solution results obtained from the proposed model formulation can accurately predict the increasing trend of experimental data related to the tank's pressure during the charging operation. The results are almost identical for 'finer' and 'extra fine' mesh sizes. Therefore, 'finer' mesh size has been chosen for further numerical calculation over the two adsorbent systems. As shown in Figure 10, the ANG vessel's pressure increases quite fast during the loading cycle. The model predictions are close to the actual pressure data measured inside the ANG bed, especially the initial points. The excellent model's ability for pressure prediction results from applying the appropriate and reality-based boundary conditions.

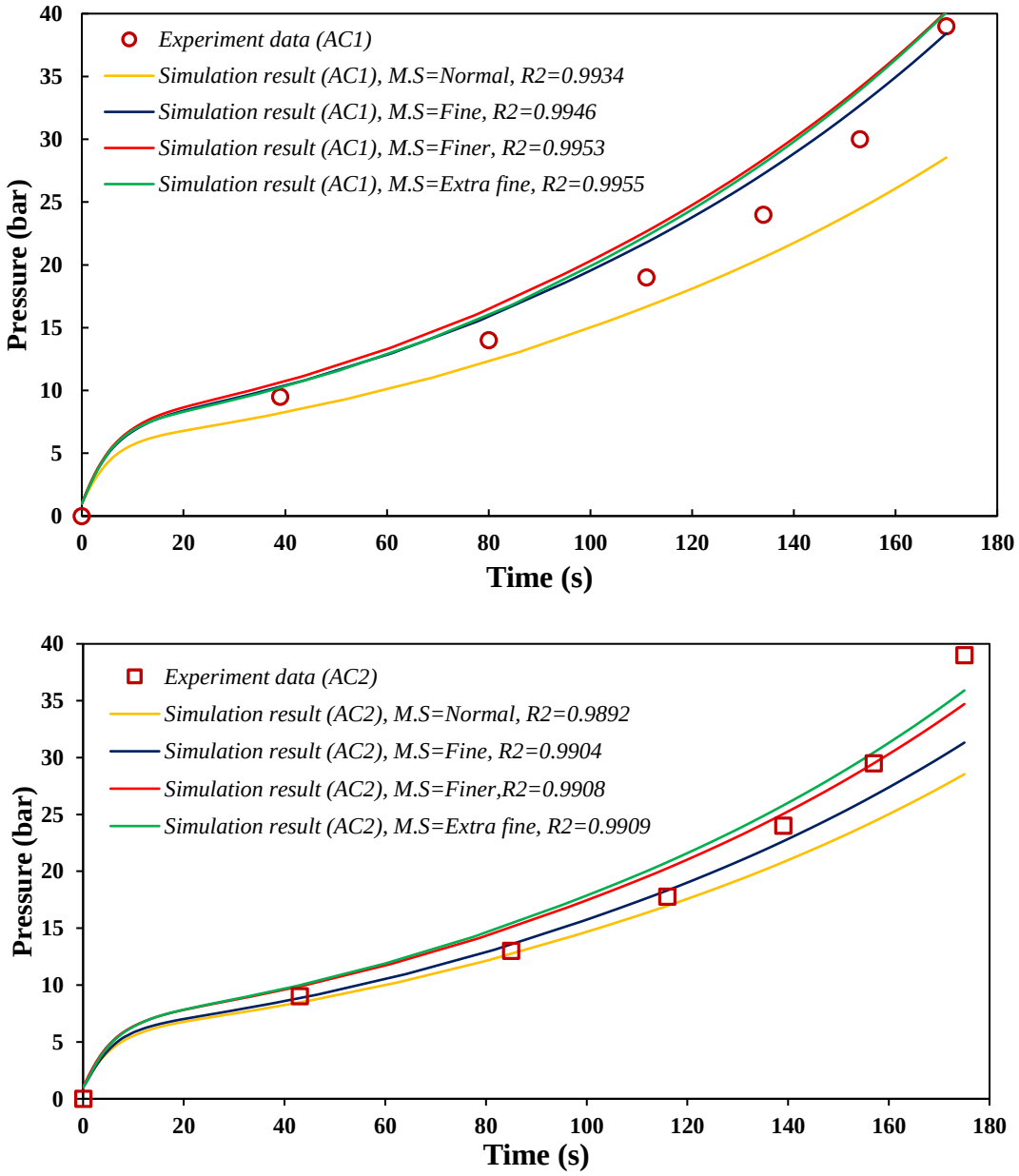

Figure 10. *Experimental data and simulation results for pressure variations inside the cylinder as a function of time during the charging process. The term M.S. denotes the mesh size.*

Figure 11 shows the simulation and the experimental temperature profiles at the centre of the ANG tank (i.e. sensors 2 and 3) as a function of time during the charging process for both AC1 and AC2 adsorbents. The experimental data and the corresponding model-predicted values for the rest of

the temperature sensors located in various axial and radial positions were illustrated in Figure S4 of the Supporting Information.

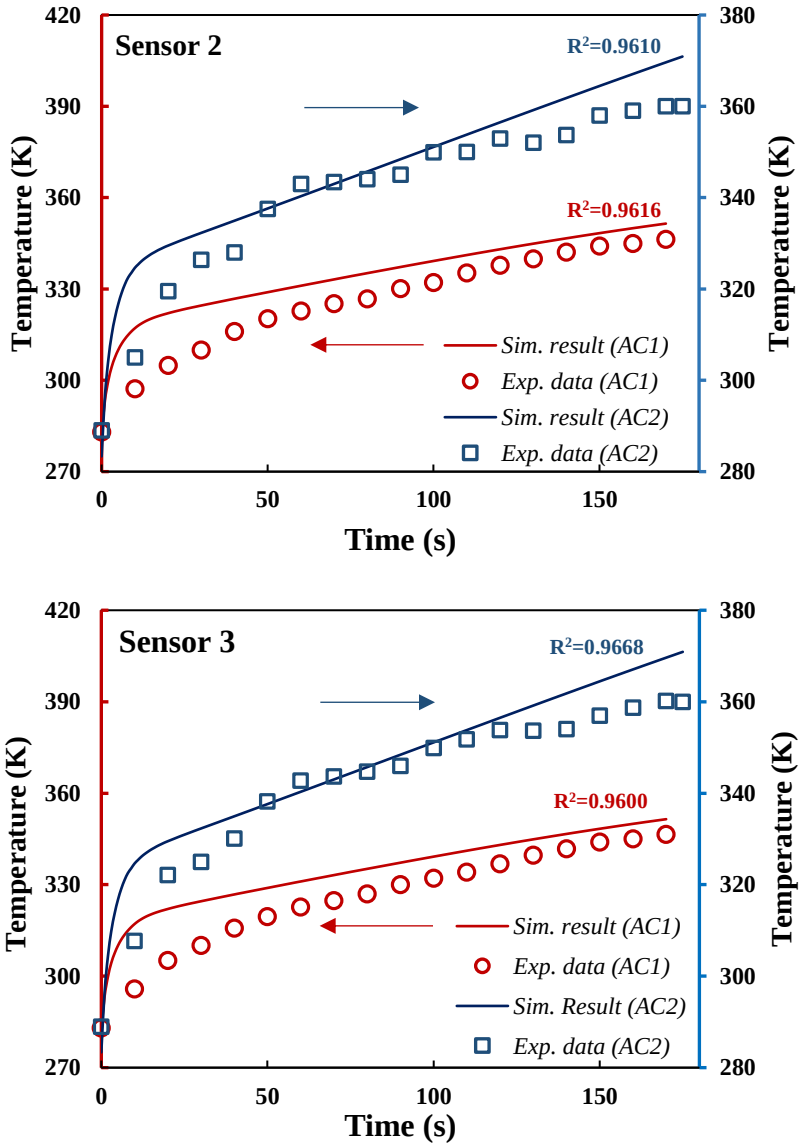

Figure 11. *Experimental data and model-predicted temperature profiles at the centre region of the ANG cylinder (i.e. sensors 2 and 3) as a function of time during the charging process.*

The overall trend of the predicted temperature change matches the experimental data though a higher temperature increase was predicted at the early stages of charging. For instance, 5.6% error, or a temperature difference of 17 K, is observed between the predicted and measured values for sensor 3 at t=20 s, when the ANG vessel is filled with AC1. The deviation of the

model's temperature prediction from the experimental data was also reported by other researchers [22, 25, 29]. One possible reason for the model deviation is the variation of the heat of adsorption during the charging process; this parameter was assumed to be a constant in the simulation. Possible experimental errors, such as miscalculation of the packing density, are other possible reasons for the deviation of the simulation and observed values. The ANG tank was filled with the adsorbents by pouring the ACs powder inside the cell, followed by pushing to ensure that the powder was softly packed. Unfortunately, there is no way of ensuring that there are no undesired voids in the packed bed.

5. Sensitivity analysis

The proposed model for the simulation of ANG vessel during the charging process is used to study the effects of two critical operating parameters of (i) geometrical configuration of ANG vessel and (ii) the specific heat capacity of the adsorbent on the entire system's thermal behaviour (at the centre of the ANG bed) and storage capacity. In each case, all the base parameters were kept constant, and only input variables of the designation of ANG bed and the specific heat capacity of the adsorbent were changed.

5.1 Effect of the geometrical configuration of the ANG vessel

Here, the impact of different L/D ratios in ANG vessels' geometrical design on their performance has been investigated. Simulations were conducted for four different geometries of (L, D), (2L, D), (L, 2D) and (2L, 2D), where L= 130 mm and D=25 mm. The values of L and D follow the dimensions of our costumed-built ANG bed described in section 3.2.

Figure 12 (A) illustrates the effect of various 2D unit dimensions and geometry on pressure variations inside the ANG bed. Although a similar trend was observed for the pressure changes in different ANG geometries, the maximum pressure limit (40 bar) has been reached within a longer time (245 s) for the largest ANG vessel (2L, 2D). In other words, increasing the diameter and length extends the ANG bed volume, which results in a longer required time for charging the bed up to the desired pressure point.

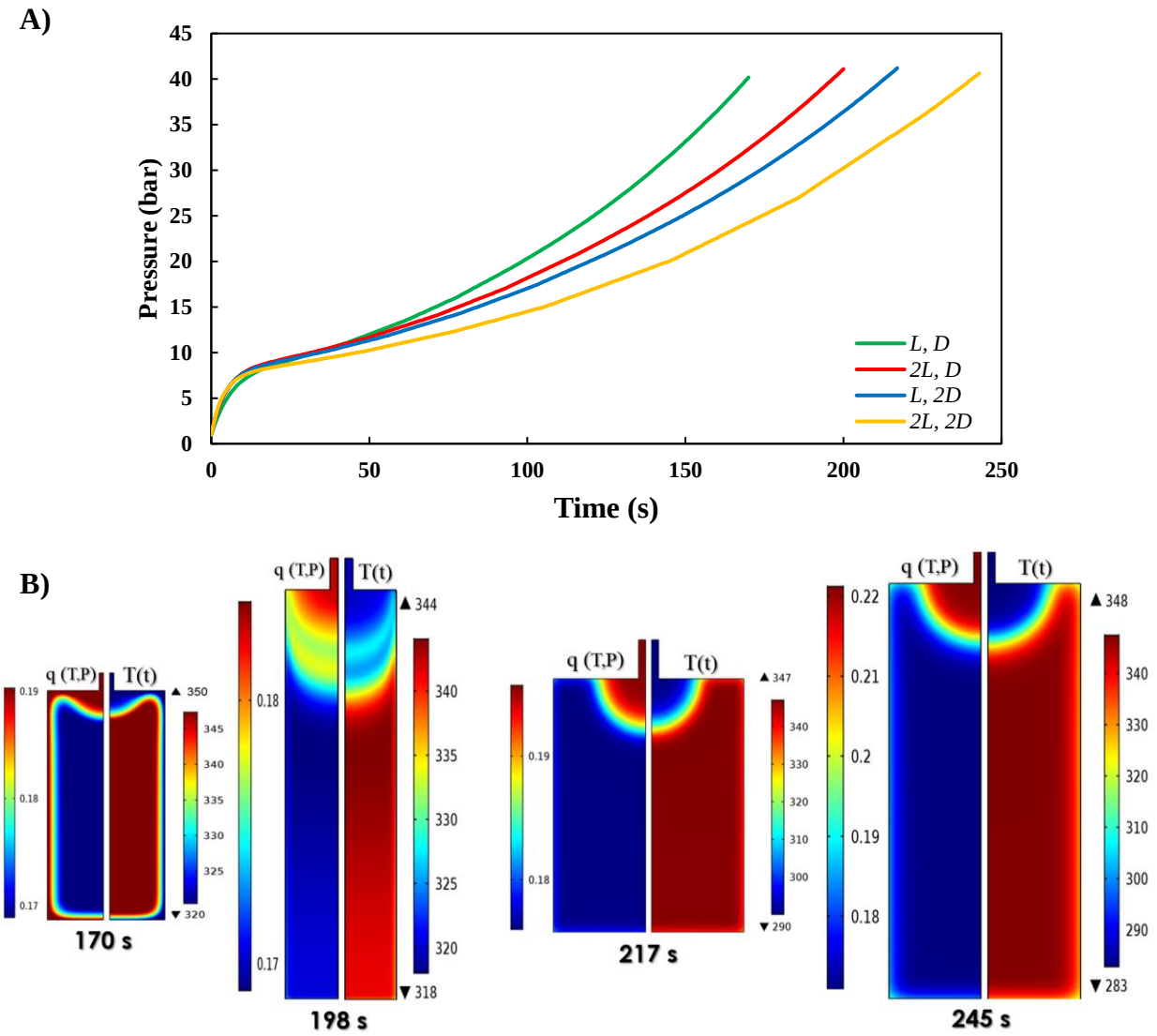

Figure 12. *(A) Effect of different ANG vessel geometries on the tank's pressure profiles, (B) Two-dimensional demonstration of the effect of different ANG vessel geometries on the thermal behaviour (T) and gravimetric storage capacity (q) at the pressure of 40 bar.*

As the two-dimensional temperature distribution curves in Figure 12 (B) show, most thermal stress is at the bed's centre in all diverse geometry designs. Amount of heat flux released inside the chamber decreases by moving from the centre towards the wall. Generally speaking, the heat transfer rate is higher around the wall than the bed's centre. Moreover, since storage efficiency is significantly affected by the bed's temperature fluctuations, the potential regions for the lowest and

highest gas uptake correspond to the ANG bed's centre and entrance, respectively [13, 15, 17, 22, 25].

5.2 Effect of specific heat capacity of adsorbents (C_p)

The adsorbent's specific heat capacity plays a significant role in controlling the temperature fluctuations and, consequently, the ANG vessel's thermal regulation [42]. Here, the effect of different adsorbent heat capacity values on ANG bed performance is studied during the charging operation. As depicted in Figure 13 (A), the bed's thermal fluctuations have been increased by decreasing the adsorbent's specific heat capacity. The minimum (45 K) and the maximum (74 K) temperature variations inside the bed are associated with the highest (1350 J/kg.K) and lowest (650 J/kg.K) C_p values, respectively. These findings agree well with those reported in the literature [12, 22, 26].

Figure 13 (B) exhibits the impact of different values of the adsorbent's heat capacity (800, 1100 and 1350 J/kg.K) on the thermal fluctuations and storage efficiency of the ANG vessel. Increasing the specific heat capacity leads to a decrease in the temperature variations inside the bed; consequently, this issue positively affects the system's gas storage efficiency. For instance, when the heat capacity rises from 800 to 1350 J/kg.K, the temperature variations are reduced to 37% and the results show the 7.7% enhancement in gravimetric methane storage efficiency within the bed.

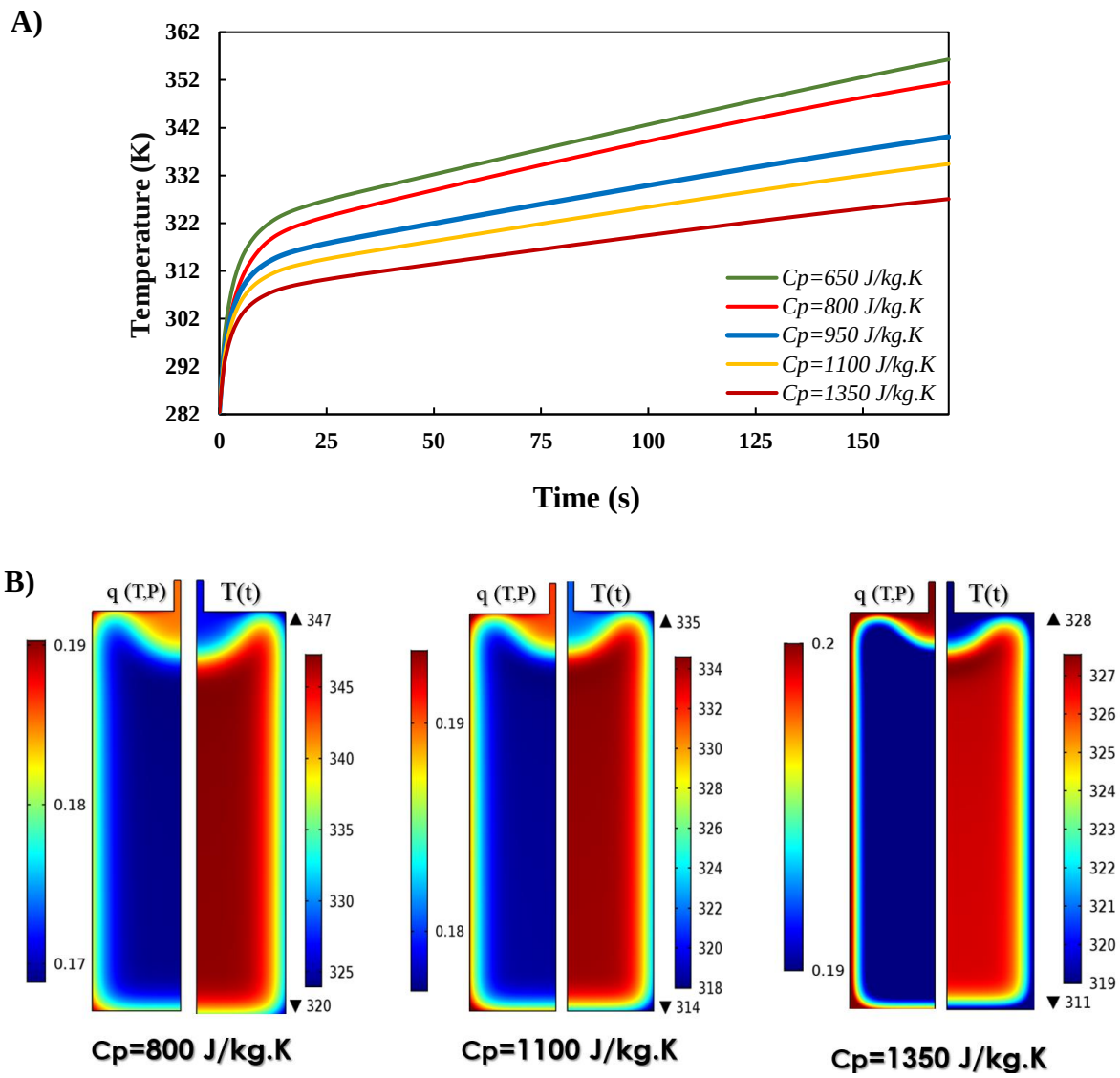

Figure 13. *(A) Effect of the adsorbent's specific heat capacity on the ANG chamber's temperature profile at the ANG bed centre. (B) Two-dimensional demonstration of the effect of adsorbent's specific heat capacity on the thermal behaviour (T) and gravimetric storage capacity (q) at the pressure of 40 bar.*

6. Conclusion

As a primary aim of the present study, we investigated the behaviour of dynamic CH_4 storage inside an ANG tank filled with carbon-based adsorbent through experimental and theoretical analysis. The variable charging flow rate was considered to mimic the actual condition when an

ANG capsule is set. The obtained experimental data of the CH_4 loading were used to validate the simulation results calculated from a 2D-distributed model, which included partial differential formulations. According to the experimental and modelling findings, the following points can be drawn:

- Due to the release of the heat of adsorption during the charging process, adsorbents' structural properties and thermal conductivity strongly influence the bed's temperature and, as a result, its efficiency.
- During continuous charging, the ANG bed temperature profiles showed a sharp increase in the first 20 seconds of dynamic CH_4 loading due to the higher rate of methane adsorption on fresh/regenerated adsorbents.
- The high-temperature profile of AC2 compared to AC1 was observed, which is attributed to their methane uptake capacity of 184 and 175 cm^3(STP)/cm^3, respectively.
- The maximum temperature rise occurred at the storage bed's central region.
- A good agreement was observed between the proposed model's and experimental pressure and temperature profiles according to numerical solution results. Superior correspondence of model prediction with collected data is the consequence of applying the appropriate and reality-based boundary conditions.
- The effect of tank geometry (L/D ratios) on the ANG performance was studied, and it was noticed that a longer time (245 s) is required for the largest studied ANG dimension (2L, 2D) to reach the maximum pressure limit (40 bar).
- Application of adsorbents with the high and low adsorbent specific heat capacity of 1350 J/kg.K and 650 J/kg.K results in a minimum (45 K) and maximum (74 K) temperature variations inside the bed, respectively.

The present study's combined theoretical and practical research could be extended for modelling ANG vessels using novel high capacity adsorbents such as MOFs and COFs PAFs and hybrid structured adsorbents. Future studies can also assess the employment of cold media such as nanofluids for circulation around the ANG vessel to improve storage operation efficiency.

7. Declaration of competing interest

All co-authors have agreed to the submission of the final manuscript and have no financial conflict of interest that might be construed to influence the results or interpretation of their manuscript.

8. Acknowledgments

This work is supported by South Pars Gas Complex (Grant Number 306494) and Ferdowsi University of Mashhad, (Grant Number 44340) for Mrs. Mirzaei provided through a Postgraduate Research Scholarship.

9. Appendix A. Supplementary Information

The Supplementary Information related to the presented article has been reported separately in the file with the same name.

References

[1] J.A. Mason, M. Veenstra, J.R. Long, Evaluating metal–organic frameworks for natural gas storage, Chemical Science 5(1) (2014) 32-51.
[2] DOE/EIA. Annual Energy Outlook 2016. 2016.
[3] S. Alhasan, R. Carriveau, D.-K. Ting, A review of adsorbed natural gas storage technologies, International Journal of Environmental Studies 73(3) (2016) 343-356.
[4] M. Smith, J. Gonzales, Costs associated with compressed natural gas vehicle fueling infrastructure, National Renewable Energy Lab.(NREL), Golden, CO (United States), 2014.
[5] J. Cho, G.J. Lim, S.J. Kim, T. Biobaku, Liquefied natural gas inventory routing problem under uncertain weather conditions, International Journal of Production Economics 204 (2018) 18-29.
[6] J. Romanos, M. Beckner, T. Rash, L. Firlej, B. Kuchta, P. Yu, G. Suppes, C. Wexler, P. Pfeifer, Nanospace engineering of KOH activated carbon, Nanotechnology 23(1) (2011) 015401.
[7] N.F. Attia, M. Jung, J. Park, H. Jang, K. Lee, H. Oh, Flexible nanoporous activated carbon cloth for achieving high H2, CH4, and CO2 storage capacities and selective CO2/CH4 separation, Chemical Engineering Journal 379 (2020) 122367.
[8] S.Y. Sawant, K. Munusamy, R.S. Somani, M. John, B.L. Newalkar, H.C. Bajaj, Precursor suitability and pilot scale production of super activated carbon for greenhouse gas adsorption and fuel gas storage, Chemical Engineering Journal 315 (2017) 415-425.
[9] S. Mirzaei, A. Ahmadpour, A. Shahsavand, A.N. Pour, L. LotfiKatooli, A.G. Asil, B. Pouladi, A. Arami-Niya, Experimental and simulation study of the effect of surface functional groups decoration on CH4 and H2 storage capacity of microporous carbons, Applied Surface Science 533 (2020) 147487.
[10] A. Sáez, M. Toledo, Thermal effect of the adsorption heat on an adsorbed natural gas storage and transportation systems, Applied thermal engineering 29(13) (2009) 2617-2623.
[11] S. Sahoo, M. Ramgopal, A simple regression equation for predicting charge characteristics of adsorbed natural gas storage systems, Applied thermal engineering 73(1) (2014) 1095-1102.

[12] D. Ybyraiymkul, K.C. Ng, A. Kaltayev, Experimental and numerical study of effect of thermal management on storage capacity of the adsorbed natural gas vessel, Applied Thermal Engineering 125 (2017) 523-531.
[13] M. Prosniewski, T. Rash, J. Romanos, A. Gillespie, D. Stalla, E. Knight, A. Smith, P. Pfeifer, Effect of cycling and thermal control on the storage and dynamics of a 40-L monolithic adsorbed natural gas tank, Fuel 244 (2019) 447-453.
[14] M. Da Silva, L. Sphaier, Dimensionless lumped formulation for performance assessment of adsorbed natural gas storage, Applied energy 87(5) (2010) 1572-1580.
[15] P. Sahoo, B. Prajwal, S.K. Dasetty, M. John, B. Newalkar, N. Choudary, K. Ayappa, Influence of exhaust gas heating and L/D ratios on the discharge efficiencies for an activated carbon natural gas storage system, Applied energy 119 (2014) 190-203.
[16] J. Yang, H. Bai, H. Shang, J. Wang, J. Li, S. Deng, Experimental and simulation study on efficient CH4/N2 separation by pressure swing adsorption on silicalite-1 pellets, Chemical Engineering Journal 388 (2020) 124222.
[17] F.N. Ridha, R.M. Yunus, M. Rashid, A.F. Ismail, Thermal analysis of adsorptive natural gas storages during dynamic charge phase at room temperature, Experimental thermal and fluid science 32(1) (2007) 14-22.
[18] J.B. Mota, A. Rodrigues, E. Saatdjian, D. Tondeur, Dynamics of natural gas adsorption storage systems employing activated carbon, Carbon 35(9) (1997) 1259-1270.
[19] L. Vasiliev, L. Kanonchik, D. Mishkinis, M. Rabetsky, Adsorbed natural gas storage and transportation vessels, International journal of thermal sciences 39(9-11) (2000) 1047-1055.
[20] K.A. RAHMAN, Experimental and theoretical studies on adsorbed natural gas storage system using activated carbons, 2011.
[21] M. Khorashadizadeh, M.N. Shahrak, A. Shahsavand, Reliable modeling of discharge process for adsorbed natural gas storage tanks, Korean Journal of Chemical Engineering 31(11) (2014) 1994-2002.
[22] K.H. Patil, S. Sahoo, Charge characteristics of adsorbed natural gas storage system based on MAXSORB III, Journal of Natural Gas Science and Engineering 52 (2018) 267-282.
[23] P.K. Sahoo, M. John, B.L. Newalkar, N. Choudhary, K. Ayappa, Filling characteristics for an activated carbon based adsorbed natural gas storage system, Industrial & engineering chemistry research 50(23) (2011) 13000-13011.
[24] S. Sahoo, M. Ramgopal, Theoretical performance of an adsorbed natural gas storage system subjected to variable charge–discharge conditions, International Journal of Ambient Energy 37(4) (2016) 372-383.
[25] M. Bastos-Neto, A.E.B. Torres, D.C. Azevedo, C.L. Cavalcante, A theoretical and experimental study of charge and discharge cycles in a storage vessel for adsorbed natural gas, Adsorption 11(2) (2005) 147-157.
[26] K.A. Rahman, W.S. Loh, A. Chakraborty, B.B. Saha, W.G. Chun, K.C. Ng, Thermal enhancement of charge and discharge cycles for adsorbed natural gas storage, Applied Thermal Engineering 31(10) (2011) 1630-1639.
[27] G.J. Van Wylen, R.E. Sonntag, C. Borgnakke, Fundamentals of classical thermodynamics, Wiley New York1976.
[28] R. Basumatary, P. Dutta, M. Prasad, K. Srinivasan, Thermal modeling of activated carbon based adsorptive natural gas storage system, Carbon 43(3) (2005) 541-549.
[29] P. Sahoo, K. Ayappa, M. John, B. Newalkar, N. Choudary, Simulation of methane adsorption in ANG storage system, Proceedings of the COMSOL Conference, 2010, pp. 2-7.
[30] K. Chang, O. Talu, Behavior and performance of adsorptive natural gas storage cylinders during discharge, Applied Thermal Engineering 16(5) (1996) 359-374.
[31] A. Shahsavand, A. Ahmadpour, Application of optimal RBF neural networks for optimization and characterization of porous materials, Computers & Chemical Engineering 29(10) (2005) 2134-2143.
[32] J. Goodling, R. Vachon, W. Stelpflug, S. Ying, M. Khader, Radial porosity distribution in cylindrical beds packed with spheres, Powder Technology 35(1) (1983) 23-29.

[33] S. Mirzaei, A. Ahmadpour, A. Shahsavand, H. Rashidi, A. Arami-Niya, A Comparative study between regression and soft computing models to maximize methane storage capacity of anthracite-based adsorbents, Industrial & Engineering Chemistry Research (2020).
[34] S.A. Mirzaei, A.; Shahsavand, A.; Rashidi, H.; Arami-Niya, A., Superior performance of modified pitch-based adsorbents for cyclic methane storage, Journal of Energy Storage (2020).
[35] COMSOL Multiphysics® v. 5.4. www.comsol.com. COMSOL AB, Stockholm, Sweden.
[36] https://en.wikipedia.org/wiki/Methane.
[37] G. Makomaski, W. Ciesińska, J. Zieliński, Thermal properties of pitch-polymer compositions and derived activated carbons, Journal of thermal analysis and calorimetry 109(2) (2012) 767-772.
[38] F. Stoeckli, A. Guillot, D. Hugi-Cleary, A. Slasli, Pore size distributions of active carbons assessed by different techniques, Carbon 38(6) (2000) 938-941.
[39] ASTM A516 / A516M-17, Standard Specification for Pressure Vessel Plates, Carbon Steel, for Moderate- and Lower-Temperature Service, ASTM International, West Conshohocken, PA, 2017, www.astm.org.
[40] D. Lozano-Castello, M. Lillo-Rodenas, D. Cazorla-Amorós, A. Linares-Solano, Preparation of activated carbons from Spanish anthracite: I. Activation by KOH, Carbon 39(5) (2001) 741-749.
[41] D.-Y. Peng, D.B. Robinson, A new two-constant equation of state, Industrial & Engineering Chemistry Fundamentals 15(1) (1976) 59-64.
[42] A. Chakraborty, B.B. Saha, S. Koyama, K. Ng, Specific heat capacity of a single component adsorbent-adsorbate system, Applied physics letters 90(17) (2007) 171902.